In Vitro Corrosion and Bioactivity Performance of Surface-Treated Ti-20Nb-13Zr Alloys for Orthopedic Applications

Madhan Kumar Arumugam [1],*, Mohamed A. Hussein [1], Akeem Yusuf Adesina [1] and Nasser Al-Aqeeli [2],*

[1] Center of Research Excellence in Corrosion, King Fahd University of Petroleum and Minerals, Dhahran 31261, Saudi Arabia; mahussein@kfupm.edu.sa (M.A.H.); adesina@kfupm.edu.sa (A.Y.A.)
[2] Department of Mechanical Engineering, King Fahd University of Petroleum and Minerals, Dhahran 31261, Saudi Arabia
* Correspondence: madhankumar@kfupm.edu.sa (M.K.A.); naqeeli@kfupm.edu.sa (N.A.-A.);
   Tel.: +96-61-3860-4818 (M.K.A.)

check for updates

Abstract: The influence of surface treatments on the microstructure, in vitro bioactivity and corrosion protection performance of newly fabricated Ti-20Nb-13Zr (TNZ) alloys was evaluated in simulated body fluid (SBF). The TNZ alloy specimens were treated with separate aqueous solutions of NaOH and H_2O_2 and with a mixture of both, followed by thermal treatment. The nanoporous network surface structure observed in H_2O_2-treated and alkali-treated specimens was entirely different from the rod-like morphology observed in alkali hydrogen peroxide-treated specimens. XRD results revealed the formation of TiO_2 and sodium titanate layers on the TNZ specimens during surface treatments. The water contact angle results implied that the surface-treated specimens exhibited improved surface hydrophilicity, which probably improved the bioactivity of the TNZ specimens. The in vitro corrosion protection performance of the surface-treated TNZ specimens was analyzed using electrochemical corrosion testing in SBF, and the obtained results indicated that the surface-treated specimens exhibited improved corrosion resistance performance compared to that of the bare TNZ specimen. The in vitro bioactivity of the treated TNZ specimens was assessed by soaking in SBF, and all the investigated treated specimens showed numerous apatite nucleation spheres within 3 days of immersion in SBF.

Keywords: Ti implants; corrosion; in vitro bioactivity; surface treatment

1. Introduction

Metallic materials, including 316L stainless steel (SS), titanium (Ti) and its alloys, and cobalt alloys are employed as orthopedic implants, which are clinically placed inside the human body to restore bone performance through strengthening or substituting an injured bone structure. Mostly, orthopedic implants are utilized as permanent or temporary medical devices depending on the fractured bone. The frequency of orthopedic fractures or illness and the increasing number of aged populations have globally driven the demand for orthopedic implants in recent years. Among the available metallic implant materials, Ti and its alloys have been the most frequently utilized orthopedic implants for the past many decades due to their good ductility, high specific strength, adequate corrosion resistance and acceptable biocompatibility [1–3]. However, the interaction of Ti implants with human bone after implantation is still considered a core concern because Ti cannot interact with bone tissues, which can further influence bone resorption, increasing the possible threat of loosening [4]. Several surface treatments and coatings have been developed in the past decades to create interactions between implants and the surrounding bone and to improve corrosion protection

performance in the physiological environment [5–7]. Enhanced corrosion and wear resistance and improved osseointegration rates with good biocompatibility are the most significant features that can be achieved through surface modification of orthopedic implants.

The surface features of implant materials play a major role in extending the service life of orthopedic implants. In general, many researchers have enthusiastically explored diverse approaches to achieve biocompatibility and the wear- and corrosion-resistant performance of metallic implants, targeting improved adaptation to the implant environment [8,9]. Hence, the surface treatment approach appears to be the most feasible alternative for enhancing the corrosion resistance and relevant features of biomaterial surfaces. Among the available methods, surface treatment by chemical methods has been widely considered owing to its ease, low cost, bone bonding capability and appropriateness for implants with complex forms [10,11]. Sodium hydroxide and hydrogen peroxide have been the most commonly utilized reagents in the surface treatment of Ti implants in recent years [12–14]. Through NaOH treatment, a sodium titanate film is generated over the Ti substrate; the potential mechanism for the initiation and evolution of hydroxyapatite on surface-modified Ti was reported by Kim et al. [14]. However, Ti alloys produce a titania gel layer with H_2O_2 treatment, and these gel layers possess a synergetic effect, inducing hydroxyapatite growth after exposure in simulated body fluid (SBF); hence, treated Ti surfaces are considered bioactive.

Ti-6Al-4V (Ti64/G5) alloys have been the most commonly employed orthopedic implants in the last few decades; however, the leaching of V and Al species from the Ti64 implant surface severely disrupts the biocompatibility of orthopedic Ti implants due to the cytotoxicity and neurotoxicity of the released ions, which additionally hinder bone mineralization. Therefore, many Ti-based alloys have been prepared to overcome the shortcomings of Ti64/G5 alloys in the orthopedic field. The author's research team recently developed a nanograined Ti-20Nb-13Zr (TNZ) alloy and investigated the in vitro corrosion resistance and biocompatibility of the developed alloy in SBF medium [15,16]. To enhance the in vitro corrosion and bioactivity of TNZ alloy, the target of this investigation is to explore the influence of surface treatment of the newly developed Ti alloy substrates on their corrosion and bioactivity performance in SBF medium.

2. Materials and Methods

2.1. Specimen Preparation

The base substrate used in the current study is a newly developed TNZ alloy fabricated by ball milling and spark plasma sintering techniques using elemental powders of Ti, Nb and Zr with 99.8% purity provided by Alfa Aesar, Haverhill, MA, USA, as explained previously [15,17]. TNZ alloy specimen discs with a diameter of 2 cm were ground using SiC grit papers from 400 to 2400 and finally polished with alumina to attain a mirror-like surface. Afterward, the specimens were washed with distilled water, ultrasonicated with acetone to remove residuals and then dried in air.

2.2. Surface Treatment

First, the TNZ alloy specimens were soaked in an acidic mixture of HNO_3:HF:H_2O (1:3:6 vol.) at 60 °C for 2 min to remove the natural oxide film; then, the specimen was washed with distilled water for 10 min and then dried in air. For alkali treatment, the TNZ specimens were immersed in 25 mL of 10 M NaOH solution at 60 °C for 24 h, cleaned with distilled water and dried at 40 °C for approximately 24 h in an air furnace. Subsequently, thermal treatment was performed by keeping specimens in an aluminum crucible at 600 °C for approximately 1 h in a muffle furnace and allowing them to cool to room temperature (RT) in the furnace. For H_2O_2 treatment, TNZ specimens were soaked in 25 mL of 10 M H_2O_2 solution at 80 °C for 1 h, and then the specimen was thermally treated at 400 °C for 1 h in an air furnace. For alkali-hydrogen peroxide treatment, the TNZ specimens were immersed in 25 mL of a mixture of 10 M NaOH and 10 M H_2O_2 at 60 °C for 1 h, and then the specimen was cleaned with distilled water and dried at 40 °C. Subsequently, the specimens were thermally treated at 600 °C for 1 h

and allowed to reach RT in the furnace. Finally, all the treated specimens were ultrasonicated with distilled water to eliminate the attached residues on the specimen surface. The alkali-, H_2O_2- and NaOH + H_2O_2 mixture-treated samples were labeled SHT, HPT and SHPT, respectively.

2.3. In Vitro Bioactivity of Surface-Treated Samples

The in vitro bioactivity of orthopedic implants is generally evaluated through the growth of hydroxyapatite on their surface during immersion in a physiological medium. Herein, the in vitro bioactivity of treated TNZ specimens was evaluated based on the procedure in previous reports [12,13]. The SBF was prepared according to a previous report [16], and then the samples were immersed in SBF for 3, 5, and 7 days. The growth of hydroxyapatite on treated TNZ specimens was examined after exposure to SBF medium for different immersion periods by SEM/EDX analysis of the treated surface.

2.4. Characterization

The surface morphology of the treated specimens was examined using field emission scanning electron microscopy (FE-SEM, Tescan microscope, Brno–Kohoutovice, Czech Republic, accelerated voltage ~20 kV and irradiation current ~10 μA). The microscale roughness of the treated specimen was measured using an optical profilometer (Contour GT-K, Bruker Nano GmbH, Billerica, MA, USA). X-ray diffraction (XRD) patterns of the treated specimen were recorded by an RINT2500 (Rigaku, Tokyo, Japan) with a scattering angle of 20°–80° at a 2θ step of 0.02°. The water contact angles (WCAs) of treated specimens were monitored using a contact angle meter (VCA OPTIMA, AST Products Inc., Billerica, MA, USA) at five different locations, and the mean was reported. After placing a drop of distilled water (10 μL) on the treated specimens, images were snapped instantly. The pictures of drops were analyzed using an image analysis system, and the contact angle (CA) was estimated from the profiles of the drops with a precision of ±0.1°.

2.5. In Vitro Corrosion-Resistant Behavior of Treated TNZ Specimens

In vitro corrosion testing was accomplished using a Gamry potentiostat/galvanostat in simulated body fluid medium. Electrochemical corrosion measurements were performed by a conventional three-electrode cell using TNZ specimens as the working electrode and a saturated calomel electrode (SCE) and a graphite rod as the reference and counter electrodes, respectively. The in vitro corrosion test was performed by monitoring the open circuit potential (OCP) for 1 h to achieve a stable state, followed by linear polarization resistance (LPR), electrochemical impedance spectroscopic (EIS) and, finally, potentiodynamic polarization (PDP) measurements. The LPR test was carried out by applying a potential of ±25 mV from the OCP with a scan rate of 0.125 mV/s. The PDP test was performed in the potential range of −250 to +1500 mV vs OCP at a scan rate of 0.196 mV/s. The electrochemical impedance spectrum was obtained in the frequency region from 100 kHz–1 mHz with an amplitude of 10 mV under the open circuit potential. The achieved EIS data were investigated using an equivalent circuit fitted through Echem Analyst software (version 6.25), which was used to calculate the chi-squared (χ^2) value to evaluate the quality of the equivalent circuit fitting. Moreover, all experiments were repeated three times for consistency.

3. Results and Discussion

3.1. Surface Characterization Results

SEM micrographs of the treated specimens are shown in Figure 1, and the treated specimens were compared using EDS analysis, shown in Figure S1 in the supporting information. The HPT specimen exhibited a cracked titanium oxide layer, which may occur during the removal of water molecules in thermal treatment. High-magnification SEM images of the HPT specimens showed a porous titania layer with homogeneously networked pores with diameters on the nanometer scale [13]. Porous nanostructures on Ti surfaces play a significant role in implant materials because an interconnected

open porous structure favors the transportation of body fluid and new bone tissue growth [18]. It has already been reported that the interaction of Ti with H_2O_2 yields a TiOOH matrix, which probably facilitates the growth of the TiO_2 layer. Furthermore, a narrowly interlinked nanoporous network is formed due to the interaction of Ti with H^+ ions from the H_2O_2 solution, leading to the relocation of the Ti and O atoms to form a thermodynamically stable and well-ordered nanostructure [19]. The SHT specimen showed a compact layer with globular-like morphology, and the corresponding EDS results revealed the existence of Ti, Nb, Zr, and O, along with Na, which further corroborated the generation of a sodium titanate layer on the TNZ specimen [20]. In general, naturally formed TiO_2 films are partially dissolved in NaOH due to corrosive OH^- ions, and the alloy specimens react with NaOH. Furthermore, hydrated TiO_2 forms negatively charged hydrates on its surface, which are then combined with sodium ions, finally forming a sodium titanate ($Na_2Ti_5O_{11}$) hydrogel film. The formed hydrogel films were dehydrated and densified to produce stable sodium titanate films during heat treatment [21].
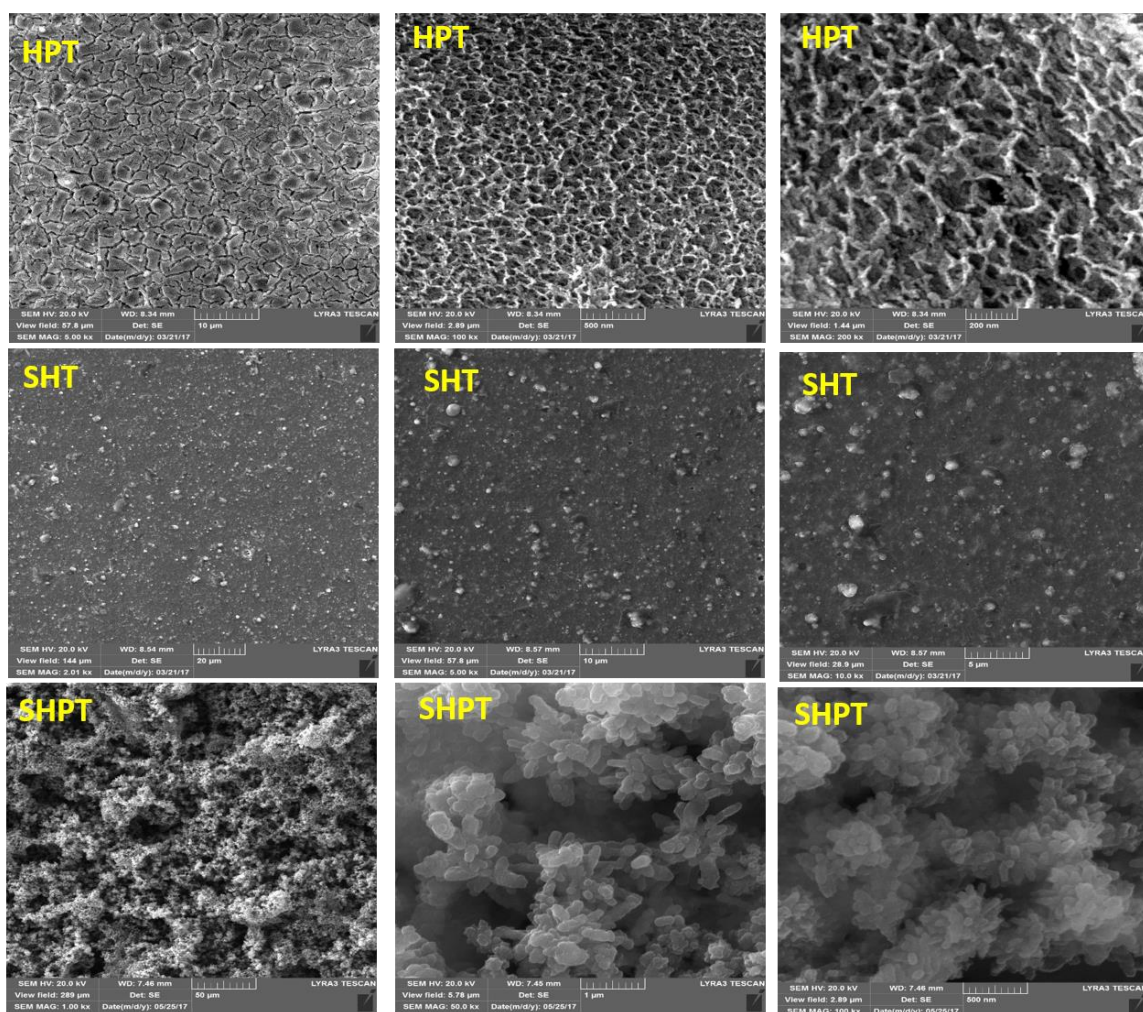

Figure 1. SEM micrographs of treated specimens.

The SHPT specimen showed a rod-like structure with agglomerated particles uniformly distributed throughout its surface. Y. Sasikumar and N. Rajendran have also reported rod-like structures with agglomerated particles on the surface of alkali- and hydrogen peroxide-treated Cp-Ti and Ti-15Mo alloy substrates [22]. It has been established that a porous nanostructure can induce bone bonding ability in the implant surface owing to the higher surface energy and large surface area in the physiological environment [23]. Lin et al. prepared different micro-/nanostructures on Ti implants and reported that

alkaline hydrothermally treated surfaces with nano-/micro nest-like and nanotube structured surfaces possessed better osseointegration ability [24].

Surface topographic images of bare and treated TNZ specimens are shown in Figure 2. In comparison with the bare TNZ specimen, all the treated specimens revealed higher surface roughness due to the formation of porous/cracked topographic surfaces. HPT specimens showed relatively heterogeneous surface topography with a distribution of pores, whereas SHT and SHPT exhibited comparatively smooth and compact surfaces with few microcracks. Recently, it has been reported that surface microroughness improves osseointegration in the initial stages and in regions of low-quality bone [25]. To obtain clearer information about surface topography, the parameters related to surface roughness were estimated from the optical profilometric images, and the obtained results are summarized in Table S1 in the supporting information. Among the parameters measured, R_a (average surface roughness) and R_q (root mean square, RMS) are considered to be more significant as these parameters indicate the magnitude of deviation from a plain surface determined by scanning a constant surface profile [26]. From Table S1, the R_q and R_a values of SHT and SHPT were lower (between 0.221–3 μm), whereas for the HPT specimen, these values were 10–40 μm. The low surface roughness values of the SHT and SHPT specimens implied a homogeneous and more compact layer compared to that of the HPT specimen. The obtained results indicated that the surface roughness parameters were influenced by the different surface modification approaches, and maximum values were observed for the HPT specimen.
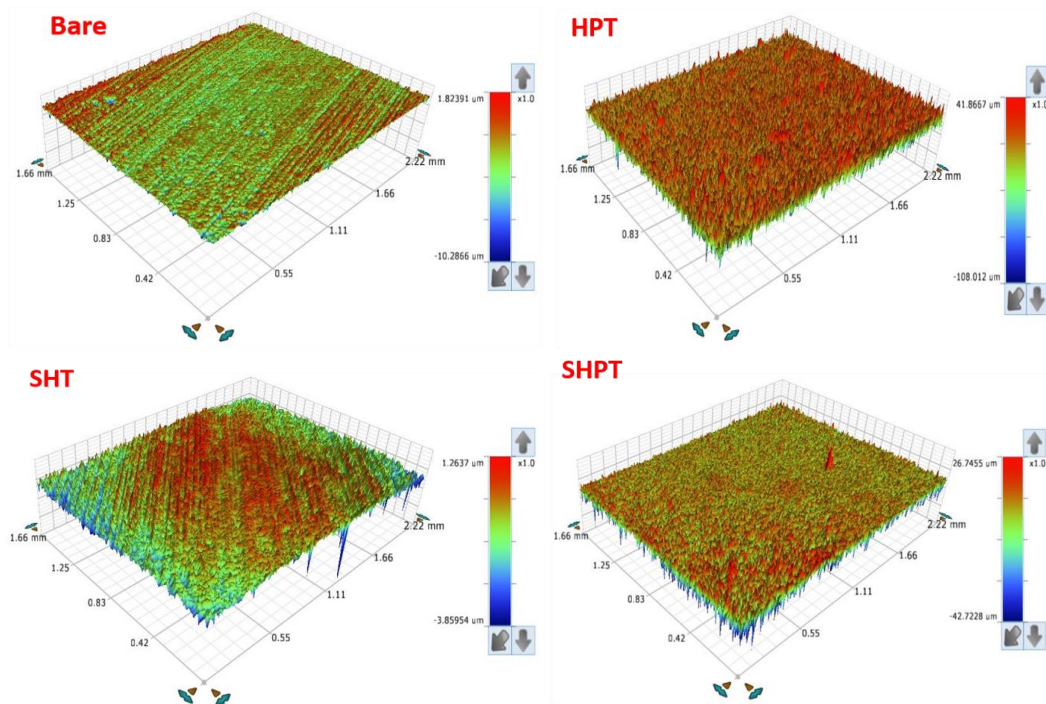

Figure 2. Surface topographic images of treated specimens.

3.2. XRD Analysis Results

Figure 3 displays the XRD patterns of surface-treated TNZ specimens. TNZ alloy is classified as a (β + α) Ti alloy, as discussed previously [15]. The peaks of the β Ti and α Ti phases of TNZ alloy were observed for all treated TNZ specimens. The SHT and SHPT specimens exhibited strong diffraction peaks at 2θ values of 36.57°, 38.25°, 42.31° and 61.6° (JCPDS No. 00-059-0666), demonstrating the generation of a sodium titanate layer on the TNZ specimens [20]. It is already well known that prismatic sodium titanate has higher crystallinity (because of subsequent thermal treatment) than alkali- and heat-treated Ti alloy [20]. HPT showed several diffraction peaks at 2θ = 23.41°, 37.85°,

45.91°, 55° and 62.55°, resulting from the (1 0 1), (0 0 4), (2 0 0) (2 1 1) and (2 0 4) planes, respectively, and representing the anatase phase of TiO$_2$. In general, the obtained anatase phase was recognized as a more appropriate phase for the generation of hydroxyapatite than the other phases [27,28].
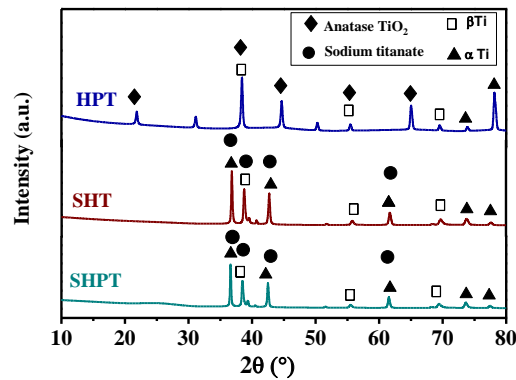

Figure 3. XRD patterns of treated specimens.

3.3. Contact Angle Results

Water contact angle (WCA) measurements were utilized to estimate the effect of surface treatment on the surface hydrophilic character of TNZ specimens, and the results are displayed in Figure 4. The WCA of the bare TNZ specimen was observed to be 88.70°, indicating its hydrophobic nature, which is in good agreement with a previous report [29]. However, for the surface-treated TNZ specimens, the obtained WCA values were lower, which confirmed the improved hydrophilicity of the surface-treated TNZ specimens. The SHPT specimen showed the lowest WCA value of 35.30°, which indicated an enhanced hydrophilic surface due to the construction of a sodium titanate film on the TNZ specimen. In general, hydrophilic surfaces on implants facilitate the growth of hydroxyapatite through ion exchange in SBF medium [30]. Pesskova et al. reported that alkali and heat treatment led to a lower contact angle and higher surface free energy by creating more OH$^-$ groups on the Ti alloy surface. These features could facilitate the adhesion of necessary proteins and improve cell attachment and proliferation [31]. Herein, the obtained results revealed that surface treatment improves the hydrophilic nature of treated TNZ specimens, which probably enhances their bioactivity.
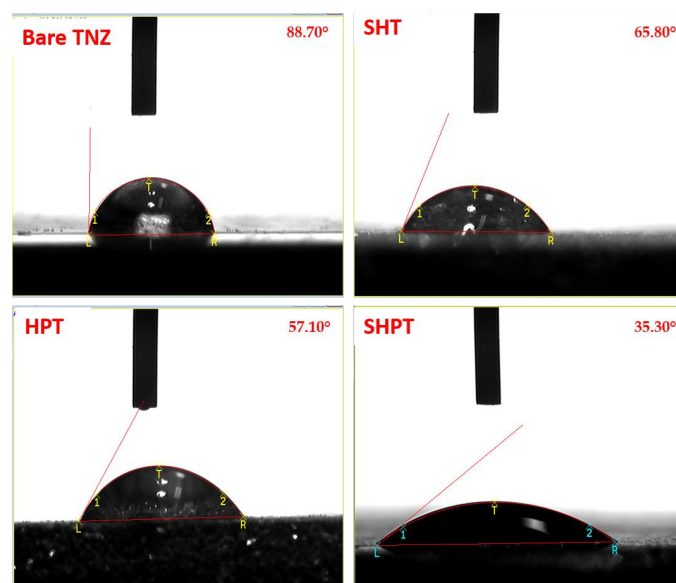

Figure 4. WCA images of treated specimens.

3.4. In Vitro Corrosion Resistance Analysis

Representative PDP curves of bare and treated TNZ specimens in SBF medium are presented in Figure 5. The electrochemical parameters extracted from the PDP curves, including the corrosion current density (I_{corr}), corrosion potential (E_{corr}), anodic and cathodic slopes (β_a and β_c), and passivation current density (I_p), are summarized in Table 1.
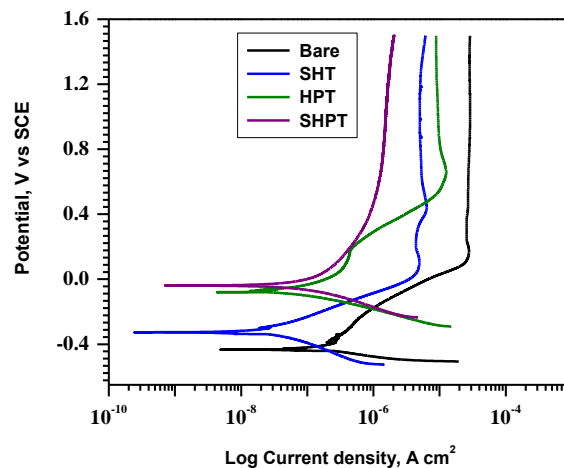

Figure 5. PDP curves of treated specimens in SBF medium.

Table 1. Tafel parameters of bare and treated TNZ specimens.

Samples	E_{corr} (V)	I_{corr} ($\mu A/cm^2$)	I_p ($\mu A/cm^2$)	β_a (mV/dec.)	β_c (mV/dec.)	Corr. Rate (mmpy) $\times 10^{-3}$
Bare	−0.443	1.012	26.051	73	92	8.880
SHT	−0.331	0.125	4.812	82	79	1.097
HPT	−0.078	0.237	9.563	74	80	2.080
SHPT	−0.031	0.091	1.312	89	78	0.8042

As the I_{corr} values extracted from Tafel analysis are smaller than the I_p values for all the investigated specimens, the TNZ surface is passive at E_{corr}. Hence, the I_{corr} values are not directly associated with the actual corrosion rates of specimens due to the existence of a passive layer on their surface; therefore, the values summarized in Table 1 can probably be utilized to acquire a comparative ranking of corrosion-resistant behavior [32]. From the observation of the PDP curves, all the investigated specimens exhibited an active-passive transition with a self-passivation region where the increase in current density against potential was nearly circumvented, revealing the formation of a stable passive layer. Generally, if the passivation current density value is lower, the metal surface tends to passivate easily [33]. Comparing the I_p values of bare and treated specimens, bare specimens showed the highest I_p values, followed by the HPT, SHT, and SHPT specimens, which implied the improved corrosion-resistant performance of TNZ specimens after surface treatment. Among the treated specimens, SHPT showed the lowest I_p values, which revealed enhanced passivation behavior in SBF. The E_{corr} values of TNZ specimens after surface treatment increased, and the I_{corr} values of TNZ specimens were noticeably lowered after surface treatment, which implied enhanced corrosion resistance in SBF medium.

In particular, the I_{corr} values of the SHPT specimen were the lowest (0.091 $\mu A/cm^2$) among the treated specimens, indicating that the mixture of NaOH and H_2O_2 solution can provide a more compact sodium titanate layer, which improved the corrosion protection performance in SBF medium.

The LPR curves of bare and treated specimens are displayed in Figure S2 in the supplementary materials. The calculated I_{corr} and polarization resistance (R_p) values are summarized in Table 2. The bare TNZ specimen exhibited an I_{corr} value of 1.264 $\mu A/cm^2$, and after surface treatment, this value

was effectively reduced, which revealed the lower corrosion rate of the treated specimens. Specifically, the I_{corr} value of SHPT (0.063 µA/cm^2) was noticeably decreased compared to those for the other treatments, emphasizing the beneficial role of the mixture of NaOH and H$_2$O$_2$ in improving the corrosion-resistant performance. In addition, the R_p value for the bare specimen was observed to be 17.67 kΩ·cm^2, whereas for the treated specimens, it was calculated to be in the range of 88–285 kΩ·cm^2. In particular, SHPT specimens showed the highest R_p value, which further corroborated the improved barrier performance of the treated specimens. From the obtained outcomes from PDP and LPR, it was preliminarily inferred that SHPT enhanced the performance of TNZ specimens in SBF medium. To attain significant evidence about the barrier performance of treated TNZ specimens in SBF medium, EIS data were recorded and are displayed in Nyquist and Bode formats in Figures 6 and 7, respectively.

Table 2. LPR parameters of bare and treated TNZ specimens.

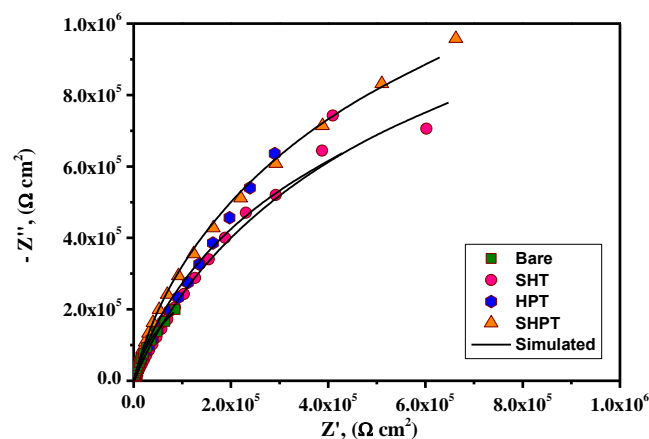| Samples	E_{corr} (V)	I_{corr} (µA/cm^2)	R_p (kΩ·cm^2)	Corr. Rate (mmpy) $\times 10^{-3}$
Bare	−0.439	1.264	17.673	11.096
SHT	−0.339	0.093	187.80	0.8164
HPT	−0.069	0.189	88.313	1.654
SHPT	−0.028	0.063	286.440	0.5534

Figure 6. Nyquist curves of treated specimens in SBF medium.
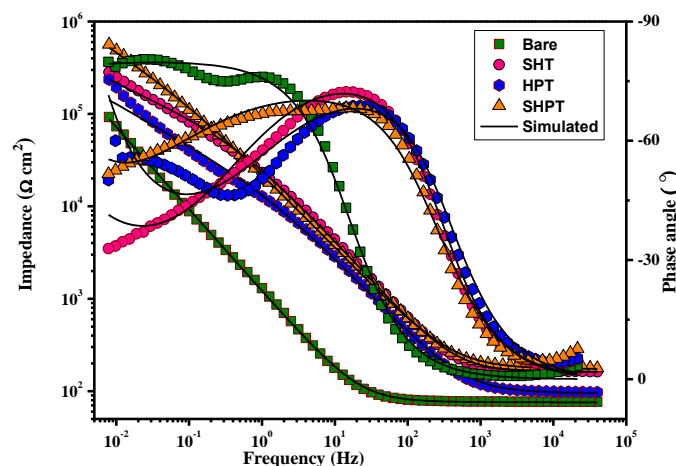

Figure 7. Bode plots of treated specimens in SBF medium.

All the investigated TNZ specimens showed a large capacitive arc in the Nyquist plots, representing the single relaxation time behavior in the investigated frequency range. In general, the diameter of the capacitive arc in the Nyquist plot is an indication of corrosion-resistant performance, and a larger

diameter denotes enhanced surface resistance against corrosion damage [34]. Comparing the Nyquist plots of bare and treated specimens, it is evident that the diameter of the capacitive arc increased; specifically, the largest diameter was observed for SHPT specimens, revealing the improved barrier performance of the formed layer during surface treatment.

Figure 7 presents the Bode plots of bare and treated TNZ specimens. No changes were observed in the impedance modulus (|Z|) at higher frequencies (10^5–10^3 Hz) due to the resistance offered by electrolytic species. On the other hand, the impedance response in the middle frequencies gives a linear relationship with a slope of almost −1, indicating the capacitive response of the treated TNZ surface. Generally, the (|Z|) value at 0.01 Hz is utilized to obtain an indication of the barrier performance of an investigated material [22,35]. For the bare specimen, the |Z| value at 0.01 Hz was found to be 80.16 $k\Omega \cdot cm^2$ in SBF medium. After surface modification, the |Z| values for SHT, HPT and SHPT were observed to be 297.29, 222.69 and 605.62 $k\Omega \cdot cm^2$, respectively.

To validate the obtained EIS data for bare and treated TNZ specimens, equivalent circuit fitting analyses were performed using suitable equivalent circuit (EC) models (Figure S3 in the supplementary materials), and the derived EIS parameters are summarized in Table 3.

Table 3. EIS parameters of bare and treated TNZ specimens.

Substrate	R_s $(\Omega \cdot cm^2)$	R_{ct} $(k\Omega \cdot cm^2)$	CPE_{dl} $(\mu F \cdot cm^{-2})$	n_{dl}	R_f $(k\Omega \cdot cm^2)$	CPE_f $(\mu F \cdot cm^{-2})$	n_f
Bare	81.24	80.16	75.41	0.94	–	–	–
SHT	78.95	297.29	1.95	0.96	12.39	14.74	0.95
HPT	80.22	222.69	2.53	0.95	11.12	18.63	0.94
SHPT	19.87	605.62	0.17	0.97	18.94	0.91	0.96

In these circuits, R_s, R_f and R_{ct} signify the electrolytic, film and charge transfer resistance, respectively. CPE_{dl} and CPE_f indicate the constant phase element of the double layer and film capacitance, respectively, which are employed to precisely fit the nonideal capacitive behavior due to the presence of defects and pores in the titanate layer. The exponent (*n*) of the constant phase element designates the deviance from perfect dielectric performance. When *n* approaches unity, the coated substrate is close to ideal capacitor behavior [36,37].

From Table 3, the R_{ct} values of the treated specimens are higher than that of the bare specimen, demonstrating the improved corrosion-resistant performance of the formed layer. In particular, SHPT specimens showed higher R_{ct} values, corroborating the beneficial role of the mixture of NaOH and H_2O_2 in forming a homogeneous and more compact surface with fewer defects [38]. In addition, the treated specimens showed a decrease in CPE_{dl} by two orders of magnitude, indicating the effective hindrance of the penetration of aggressive species (Cl^-) from the SBF medium [39]. Hence, the beneficial role of surface treatment, especially the improvement in SHPT over the TNZ specimen in terms of in vitro corrosion resistant behavior, is reflected in the higher capacitive arcs, higher R_{ct}, lower CPE_{dl}, highest E_{corr} and lower I_{corr} values. The obtained results confirm that the formation of a homogeneous and compact titanate layer improves the corrosion-resistant behavior of the TNZ surface in SBF medium.

3.5. In Vitro Characterization in SBF Medium

To estimate the in vitro bioactivity of treated TNZ specimens, the surface morphologies of treated specimens after immersion in SBF medium for 3, 5 and 7 days were determined and are displayed in Figure 8. In a previous study, we evaluated the growth of hydroxyapatite on bare TNZ specimens and reported that $Ca_3(PO_4)_2$ was formed on the entire TNZ surface after 14 days of exposure in SBF medium [16]. Herein, after 3 days of immersion in SBF, all of the treated TNZ specimens exhibited a uniform distribution of globular crystallites covering the entire surface. This growth was enhanced with prolonged immersion time, and finally, some agglomeration of particles was observed after 7 days of immersion in SBF medium.
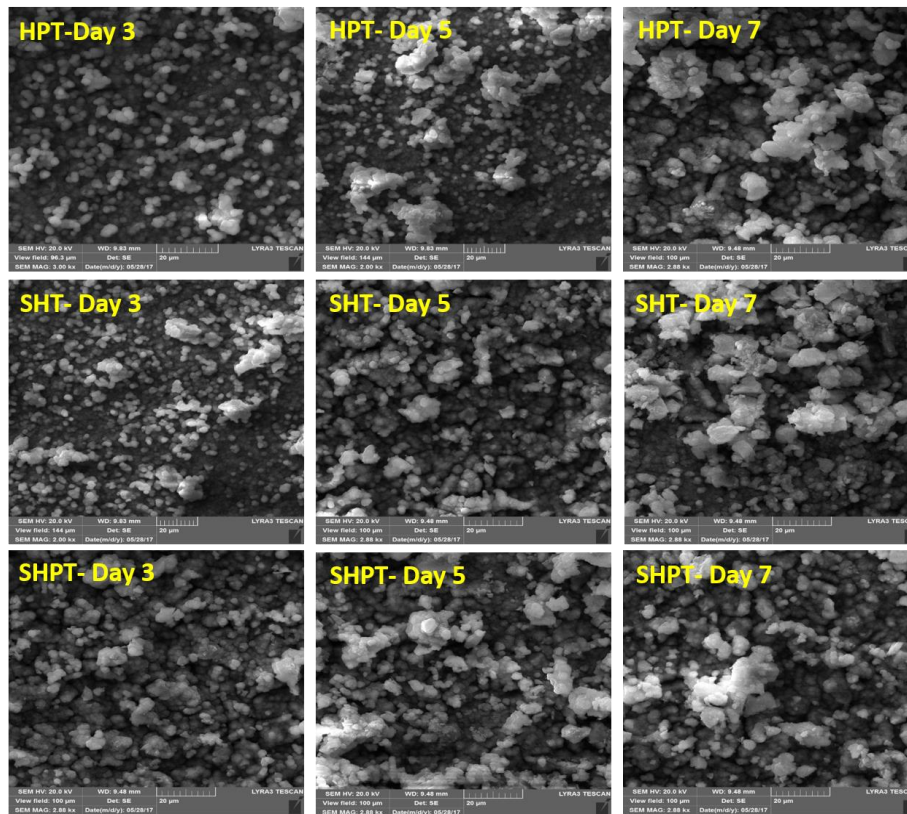
Figure 8. SEM images of treated specimens after immersion in SBF medium.

It has already been established that the formation of apatite occurs through ion exchange between the formed sodium titanate layer and SBF solution, and the mechanism and growth of apatite on treated Ti alloy have been well discussed in the literature [40,41]. Absorbed OH^- ions on the treated TNZ surface could considerably enhance the possible apatite formation on the alloy surface. Released sodium ions from the sodium titanate film increased the local pH near the specimen surface. The negative charges from $HTiO_3^-$ probably attracted Ca^{2+} (or Ca^{2+}) ions by Coulombic force and HPO_4^{2-} ions by hydrogen bonds, causing the ions to accumulate near the Ti surface. This accumulation of ions enhanced the local supersaturation degree with respect to apatite. When apatite nuclei were formed, they might spontaneously grow by consuming Ca^{2+}, HPO_4^{2-} and OH^- ions from the SBF solution [42]. Although all the treated TNZ specimens stimulated the nucleation of apatite within 3 days of exposure in SBF, the density and homogeneous distribution of apatite formed in specimens was determined to increase in the order of HPT, SHT and SHPT. The surface treatment of Ti–13Nb–13Zr alloy using anodization, alkali and H_2O_2 treatment, etc., efficiently stimulated the attachment of Ca^{2+} and HPO_4^{2-} ions or the formation of apatite, resulting in enhanced corrosion protection behavior and osseointegration capability [43–45]. The chemical composition of the obtained layer was analyzed using EDS analysis, and the results are displayed in Figure S4 in the supporting information. The presence of Ca, P and O together with the main alloying elements of TNZ specimens (Nb and Zr) was observed in the EDS spectra of treated TNZ specimens after immersion in SBF. In addition, the ratios of Ca/P for the treated TNZ specimens after exposure for 3, 5, and 7 days were found to be 1.53, 1.61, and 1.65, respectively. An increase in Ca/P ratio is usually related to the transformation of dicalcium phosphate (DCPA) into hydroxyapatite (HA) [46].

4. Conclusions

Surface treatment using chemicals and a thermal route was performed on newly developed TNZ specimens to improve their in vitro corrosion resistance and bioactivity in SBF medium. Surface

structure and microstructure characterization results from surface profilometry, SEM/EDS, and XRD implied that the SHT and SHPT specimens are characterized by a more compact sodium titanate layer on the TNZ surface, whereas the HPT specimen showed a porous network titania layer with higher surface roughness. The WCA results indicated the improved surface hydrophilicity of the treated TNZ surfaces, which may favor the in vitro bioactivity of these specimens. The in vitro corrosion performance of treated specimens in SBF medium is reflected in the higher capacitive arcs, higher R_{ct} values, lower CPE_{dl}, higher E_{corr} and lower I_{corr}. This observation validates that the formation of a homogeneous and more compact titanate layer improves the corrosion-resistant behavior of TNZ surfaces in SBF medium. Surface characterization of the treated specimens after immersion in SBF medium indicated the uniform distribution of hydroxyapatite particles on the treated TNZ specimens, which validated their in vitro bioactive performance in SBF medium.

Supplementary Materials: The following are available online at http://www.mdpi.com/2079-6412/9/5/344/s1, Figure S1: EDS analysis of bare and surface treated TNZ specimens, Table S1: Surface roughness parameters of bare and treated TNZ specimens, Figure S2: LPR curves of (a) Bare, (b) SHT, (c) HPT and (d) SHPT, Figure S3: EIS circuit models of (a) Bare and (b) treated TNZ substrates, Figure S4: EDS results of bare and surface treated substrates.

References

1. Eisenbarth, E.; Velten, D.; Müller, M.; Thull, R.; Breme, J. Biocompatibility of β stabilizing elements of titanium alloys. *Biomaterials* **2004**, *25*, 5705–5713. [CrossRef]
2. Niinomi, M. Recent research and development in titanium alloys for biomedical applications and healthcare goods. *Sci. Technol. Adv. Mater.* **2003**, *4*, 445–454. [CrossRef]
3. Geetha, M.; Singh, A.K.; Asokamani, R.; Gogia, A.K. Ti based biomaterials, the ultimate choice for orthopaedic implants—A review. *Prog. Mater. Sci.* **2009**, *54*, 397–425. [CrossRef]
4. Chen, Q.; Thouas, G.A. Metallic implant biomaterials. *Mater. Sci. Eng. R Rep.* **2015**, *87*, 1–57. [CrossRef]
5. Asri, R.; Harun, W.; Samykano, M.; Lah, N.; Ghani, S.; Tarlochan, F.; Raza, M.A. Corrosion and surface modification on biocompatible metals: A review. *Mater. Sci. Eng. C* **2017**, *77*, 1261–1274. [CrossRef]
6. Rafieerad, A.R.; Ashra, M.R.; Mahmoodian, R.; Bushroa, A.R. Surface characterization and corrosion behavior of calcium phosphate-base composite layer on titanium and its alloys via plasma electrolytic oxidation: A review paper. *Mater. Sci. Eng. C* **2015**, *57*, 397–413. [CrossRef]
7. Mohammed, M.T.; Khan, Z.K.; Siddique, A.N. Surface modifications of titanium materials for developing corrosion behavior in human body environment: A review. *Procedia Mater. Sci.* **2014**, *6*, 1610–1618. [CrossRef]
8. Hussein, M.A.; Mohammed, A.S.; Al-Aqeeli, N. Wear characteristics of metallic biomaterials: A review. *Materials* **2015**, *8*, 2749–2768. [CrossRef]
9. Geetha, M.; Dhinasekaran, D.; Rajamanickam, A. Biomedical implants: Corrosion and its prevention—A review. *Recent Pat. Corros. Sci.* **2010**, *2*, 40–54.
10. Butev, E.; Esen, Z.; Bor, S. In vitro bioactivity investigation of alkali treated Ti6Al7Nb alloy foams. *Appli. Sur. Sci.* **2015**, *327*, 437–443. [CrossRef]
11. Shukla, A.K.; Balasubramaniam, R. Effect of surface treatment on electrochemical behavior of CPTi, Ti–6Al–4V and Ti–13Nb–13Zr alloys in simulated human body fluid. *Corros. Sci.* **2006**, *48*, 1696–1720. [CrossRef]
12. Tamilselvi, S.; Raghavendran, H.B.; Srinivasan, P.; Rajendran, N. In vitro and in vivo studies of alkali- and heat-treated Ti–6Al–7Nb and Ti–5Al–2Nb–1Ta alloys for orthopedic implants. *J. Biomed. Mater. Res. A* **2009**, *90*, 380–386. [CrossRef] [PubMed]

13. Karthega, M.; Nagarajan, S.; Rajendran, N. In vitro studies of hydrogen peroxide treated titanium for biomedical applications. *Electrochim. Acta* **2010**, *55*, 2201–2209. [CrossRef]

14. Kim, H.M.; Miyaji, F.; Kokubo, T.; Nakamura, T. Effect of heat treatment on apatite forming ability of Ti metal induced by alkali treatment. *J. Mater. Sci. Mater. Med.* **1997**, *8*, 341–347. [CrossRef]

15. Hussein, M.A.; Suryanarayana, C.; Al-Aqeeli, N. Fabrication of nano-grained Ti–Nb–Zr biomaterials using spark plasma sintering. *Mater. Des.* **2015**, *87*, 693–700. [CrossRef]

16. Hussein, M.; Kumar, M.; Drew, R.; Al-Aqeeli, N. Electrochemical corrosion and in vitro bioactivity of nano-grained biomedical Ti-20Nb-13Zr alloy in a simulated body fluid. *Materials* **2018**, *11*, 26. [CrossRef] [PubMed]

17. Hussein, M.A.; Al-Aqeeli, N. Titanium Alloys for Biomedical Applications and Fabrication Methods Thereof. U.S. Patent 9828655B2, 28 November 2017.

18. Wang, X.J.; Li, Y.C.; Xiong, J.Y.; Hodgson, P.D.; Wen, C.E. Porous TiNbZr alloy scaffolds for biomedical applications. *Acta Biomater.* **2009**, *5*, 3616–3624. [CrossRef]

19. Karthega, M.; Rajendran, N. Formation of nanoporous oxide layer over a binary β-phase titanium in simulated body fluid. *J. Porous Mater.* **2012**, *19*, 573–577. [CrossRef]

20. Kumar, A.M.; Sudhagar, P.; Ramakrishna, S.; Kang, Y.S.; Kim, H.; Gasem, Z.M.; Rajendran, N. Evaluation of chemically modified Ti–5Mo–3Fe alloy surface: Electrochemical aspects and in vitro bioactivity on MG63 cells. *Appli. Surf. Sci.* **2014**, *307*, 52–61. [CrossRef]

21. Gao, Z.; Li, Q.; He, F.; Huang, Y.; Wan, Y. Mechanical modulation and bioactive surface modification of porous Ti–10Mo alloy for bone implants. *Mater. Des.* **2012**, *42*, 13–20. [CrossRef]

22. Sasikumar, Y.; Rajendran, N. Influence of surface modification on the apatite formation and corrosion behavior of Ti and Ti-15Mo alloy for biomedical applications. *Mater. Chem. Phy.* **2013**, *138*, 114–123. [CrossRef]

23. Kumar, A.M.; Hussein, M.A.; Adesina, A.Y.; Ramakrishna, S.; Al-Aqeeli, N. Influence of surface treatment on PEDOT coatings: Surface and electrochemical corrosion aspects of newly developed Ti alloy. *RSC Adv.* **2018**, *8*, 19181–19195. [CrossRef]

24. Lin, L.; Wang, H.; Ni, M.; Rui, Y.; Cheng, T.Y.; Cheng, C.K.; Pan, X.; Li, G.; Lin, C. Enhanced osseointegration of medical titanium implant with surface modifications in micro/nanoscale structures. *J. Ortho. Trans.* **2014**, *2*, 35–42.

25. Lai, Y.K.; Lin, C.J.; Wang, H.; Huang, J.Y.; Zhuang, H.F.; Sun, L. Superhydrophilic/ superhydrophobic micro pattern on TiO$_2$ nanotube films by photocatalytic lithography. *Electrochem. Commun.* **2008**, *10*, 387–391. [CrossRef]

26. Bo, A.; Zhan, H.; Bell, J.; Zhu, H.; Gu, Y. Mechanical bending properties of sodium titanate nanowires. *RSC Adv.* **2014**, *4*, 56970–56976. [CrossRef]

27. Karthega, M.; Rajendran, N. Hydrogen peroxide treatment on Ti–6Al–4V alloy: A promising surface modification technique for orthopaedic application. *Appli. Sur. Sci.* **2010**, *256*, 2176–2183. [CrossRef]

28. Wu, W.; Nancollas, G.H. Kinetics of heterogeneous nucleation of calcium phosphates on anatase and rutile. *J. Colloid Interface Sci.* **1998**, *199*, 206–211. [CrossRef]

29. Kumar, A.M.; Adesina, A.Y.; Hussein, M.A.; Ramakrishna, S.; Al-Aqeeli, N.; Akhtar, S.; Saravanan, S. PEDOT/FHA nanocomposite coatings on newly developed Ti-Nb-Zr implants: Biocompatibility and surface protection against corrosion and bacterial infections. *Mater. Sci. Eng. C* **2019**, *98*, 482–495. [CrossRef]

30. Kilpadi, D.V.; Lemons, J.E. Surface energy characterization of unalloyed Ti implants. *J. Biomed. Mater. Res.* **1994**, *28*, 1419–1425. [CrossRef]

31. Pesskova, V.; Kubies, D.; Hulejova, H.; Himmlova, L. The influence of implant surface properties on cell adhesion and proliferation. *J. Mater. Sci. Mater. Med.* **2007**, *18*, 465–473. [CrossRef]

32. Chelariu, R.; Bolat, G.; Izquierdo, J.; Mareci, D.; Gordin, D.M.; Gloriant, T.; Souto, R.M. Metastable beta Ti-Nb-Mo alloys with improved corrosion resistance in saline solution. *Electrochim. Acta* **2014**, *137*, 280–289. [CrossRef]

33. Hussein, M.A.; Azeem, M.; Kumar, A.M.; Al-Aqeeli, N.; Ankah, N.K.; Sorour, A.A. Influence of thermal treatment on the microstructure, mechanical properties, and corrosion resistance of newly developed Ti20Nb13Zr biomedical alloy in a simulated body environment. *J. Mater. Eng. Perform.* **2019**, *28*, 1337–1350. [CrossRef]

34. Hussein, M.A.; Kumar, A.M.; Yilbas, B.S.; Al-Aqeeli, N. laser nitriding of the newly developed Ti-20Nb-13Zr at.% biomaterial alloy to enhance its mechanical and corrosion properties in simulated body fluid. *J. Mater. Eng. Perform.* **2017**, *26*, 5553–5562. [CrossRef]

35. Akhtar, S.; Matin, A.; Kumar, A.M.; Ibrahim, A.; Laoui, T. Enhancement of anticorrosion property of 304 stainless steel using silane coating. *Appli. Surf. Sci.* **2018**, *440*, 286–1297. [CrossRef]

36. Hussein, M.A.; Yilbas, B.; Kumar, A.M.; Drew, R.; Al-Aqeeli, N. Influence of Laser nitriding on the surface and corrosion properties of Ti-20Nb-13Zr alloy in artificial saliva for dental applications. *J. Mater. Eng. Perform.* **2018**, *27*, 4655–4664. [CrossRef]

37. Kumar, A.M.; Babu, R.S.; Obot, I.B.; Adesina, A.Y.; Ibrahim, A.; de Barros, A.L.F. Promising hard carbon coatings on Cu substrates: Corrosion and tribological performance with theoretical aspect. *J. Mater. Eng. Perform.* **2018**, *27*, 2306–2316. [CrossRef]

38. Sasikumar, Y.; Rajendran, N. Surface modification and in vitro characterization of Cp-Ti and Ti-5Al-2Nb-1Ta alloy in simulated body fluid. *J. Mater. Eng. Perform.* **2012**, *21*, 2177–2187. [CrossRef]

39. Chen, X.B.; Li, Y.C.; Hodgson, P.D.; Wen, C. The importance of particle size in porous titanium and nonporous counterparts for surface energy and its impact on apatite formation. *Acta Biomater.* **2009**, *5*, 2290–2302. [CrossRef]

40. Chen, X.B.; Li, Y.C.; Plessis, J.D.; Hodgson, P.D.; Wen, C.E. Influence of calcium ion deposition on apatite-inducing ability of porous titanium for biomedical applications. *Acta Biomater.* **2009**, *5*, 1808–1820. [CrossRef]

41. Xiong, J.; Li, Y.; Wang, X.; Hodgson, P.; Wen, C.E. Mechanical properties and bioactive surface modification via alkali-heat treatment of a porous Ti–18Nb–4Sn alloy for biomedical applications. *Acta Biomater.* **2008**, *4*, 1963–1968. [CrossRef]

42. Simka, W. Preliminary investigations on the anodic oxidation of Ti–13Nb–13Zr alloy in a solution containing calcium and phosphorus. *Electrochim. Acta* **2011**, *56*, 9831–9837. [CrossRef]

43. Pan, J.; Liao, H.; Leygraf, C.; Thierry, D.; Li, J. Variation of oxide films on titanium induced by osteoblast-like cell culture and the influence of an H_2O_2 pretreatment. *J. Biomed. Mater. Res.* **1998**, *40*, 244–256. [CrossRef]

44. Baker, M.A.; Assis, S.L.; Grilli, R.; Costa, I. Investigation of the electrochemical behavior and surface chemistry of a Ti–13Nb–13Zr alloy exposed in MEM cell culture media with and without the addition of H_2O_2. *Surf. Interface Anal.* **2008**, *40*, 220–224. [CrossRef]

45. Sasikumar, Y.; Kumar, A.M.; Babu, R.S.; Rahman, M.M.; Samyn, L.M.; de Barros, A.L.F. Biocompatible hydrophilic brushite coatings on AZX310 and AM50 alloys for orthopaedic implants. *J. Mater. Sci. Mater. Medi.* **2018**, *29*, 123–137. [CrossRef] [PubMed]

46. Kumar, A.M.; Hassan, S.F.; Sorour, A.A.; Paramsothy, M.; Gupta, M. Investigation on the controlled degradation and in vitro mineralization of carbon nanotube reinforced AZ31 nanocomposite in simulated body fluid. *Met. Mater. Inter.* **2019**, *25*, 105–116. [CrossRef]